Cerebral Cortex, December 2020;30: 6152–6168

doi: 10.1093/cercor/bhaa170
Advance Access Publication Date: 27 June 2020
Original Article

ORIGINAL ARTICLE

White Matter Development from Birth to 6 Years of Age: A Longitudinal Study

Rebecca L. Stephens[1,*], Benjamin W. Langworthy[2], Sarah J. Short[3], Jessica B. Girault[1,4], Martin A. Styner[1,5] and John H. Gilmore[1]

[1]Department of Psychiatry, University of North Carolina at Chapel Hill, Chapel Hill, NC 27599, USA, [2]Department of Biostatistics, University of North Carolina at Chapel Hill, Chapel Hill, NC 27599, USA, [3]Department of Educational Psychology, Center for Healthy Minds, University of Wisconsin, Madison, Madison, WI 53703, USA, [4]Carolina Institute for Developmental Disabilities, University of North Carolina at Chapel Hill, Chapel Hill, NC 27599, USA and [5]Department of Computer Science, University of North Carolina at Chapel Hill, Chapel Hill, NC 27599, USA

*Address correspondence to Rebecca L. Stephens, University of North Carolina at Chapel Hill, CB #7160 Medical Wing C, Chapel Hill, NC 27599, USA. Email: rebsteph@live.unc.edu

Abstract

Human white matter development in the first years of life is rapid, setting the foundation for later development. Microstructural properties of white matter are linked to many behavioral and psychiatric outcomes; however, little is known about when in development individual differences in white matter microstructure are established. The aim of the current study is to characterize longitudinal development of white matter microstructure from birth through 6 years to determine when in development individual differences are established. Two hundred and twenty-four children underwent diffusion-weighted imaging after birth and at 1, 2, 4, and 6 years. Diffusion tensor imaging data were computed for 20 white matter tracts (9 left–right corresponding tracts and 2 commissural tracts), with tract-based measures of fractional anisotropy and axial and radial diffusivity. Microstructural maturation between birth and 1 year are much greater than subsequent changes. Further, by 1 year, individual differences in tract average values are consistently predictive of the respective 6-year values, explaining, on average, 40% of the variance in 6-year microstructure. Results provide further evidence of the importance of the first year of life with regard to white matter development, with potential implications for informing early intervention efforts that target specific sensitive periods.

Key words: diffusion tensor imaging, early childhood, infancy, white matter

Introduction

Research on early brain development has long suggested the importance of infancy and early childhood as a window of substantial changes in both brain structure and function. Advances in magnetic resonance imaging (MRI) technology has allowed for a detailed characterization of these structural changes in regard to gray and white matter. Although both gray and white matter are important for overall brain function, white matter development is intrinsically linked with changes in the brain's efficiency, which is related to a variety of cognitive, behavioral, and psychopathological outcomes (e.g., Nagy et al. 2004; Mabbott et al. 2006; Fields 2008; Filley and Fields 2016). The maturation of white matter is thought to occur alongside the early development of a number of important cognitive and behavioral functions. Individual differences in white matter microstructure are related to these outcomes as well as to risk for psychiatric illness. Specifically, a number of neuropsychiatric disorders, many thought to originate early in development, are characterized by aberrant white matter connectivity (Thomason and Thompson 2011).

A number of neurobiological mechanisms contribute to early white matter development, such as axon myelination and growth, all serving to increase the overall efficiency of these connections. Previous research on early white matter development points to the first few years of life as a time of rapid and profound growth (Knickmeyer et al. 2008; Dubois et al. 2014; Qiu et al. 2015; Lebel and Deoni 2018). The rate of development during this window underlies a higher degree of plasticity and supports the importance of this age range for setting the stage for later healthy development. In order to better understand the effects of white matter abnormalities or atypicalities, it is important to first understand typical patterns of development. Only then can we more accurately determine when abnormalities may first arise or be detected. As such, there is substantial value in improving our understanding of individual differences in typical white matter development using longitudinal designs and large samples.

The majority of research exploring trajectories of white matter microstructure development focuses on either infancy and toddlerhood or childhood through adulthood. In fact, many review articles center around these ranges, looking at either birth to 2 years (Dubois et al. 2014; Qiu et al. 2015) or ages 4 years through adulthood (Lebel et al. 2019). Missing is the research that connects the rapid development observed in the first 2 years to the relatively more stable changes occurring in early childhood. Additionally, much of the existing research is cross-sectional, and the lack of within-subject data limits the extent to which we can gain a strong understanding of individual differences in development. Even the research that is characterized as longitudinal could be more accurately described as cohort sequential or accelerated longitudinal designs (e.g., Lebel and Beaulieu 2011; Paydar et al. 2014; Simmonds et al. 2014; Krogsrud et al. 2016), which have the potential to be impacted by cohort effects. Though these studies cover a larger range of ages, they do not provide within-subject information across the full longitudinal timeframe. These studies that focus on the general trajectory of white matter development (i.e., group averages) lack an exploration of predictive ability that could be better understood by examining individual differences in development.

Changes in white matter have been characterized primarily using diffusion tensor imaging (DTI) techniques, which provide indirect measures of white matter microstructure and organization by considering the diffusion of water molecules. Diffusion characteristics reflect changes in white matter structure related to fiber organization, membrane proliferation, and fiber myelination, and DTI processing produces quantitative measures that have been demonstrated as sensitive to reliable age- and maturity-related changes (Feldman et al. 2010; Dubois et al. 2014; Tamnes et al. 2017).

White matter microstructure continues to develop across the lifespan. Although specific methodology varies between studies, this relatively large body of research has established a few consistent patterns that have been discussed in review articles (e.g., Dubois et al. 2014; Qiu et al. 2015; Lebel et al. 2019). For example, white matter development is nonlinear, with changes in the first few years being much more rapid than those in the second year and beyond (Knickmeyer et al. 2008; Gao et al. 2009; Geng et al. 2012; Gilmore et al. 2018; Girault et al. 2019). After this period, rates slow but there is continued growth at different rates across different areas of the brain. For example, some research has found that association tracts with frontal connections mature more slowly than do projection or commissural tracts (Kinney et al. 1988; Guillery 2005; Gao et al. 2009; Deoni et al. 2011, 2012; Geng et al. 2012; Lebel et al. 2019).

The goal of the current study was to fill this gap by describing the development of white matter microstructure in tracts important for cognitive development in a large, longitudinal sample from birth through 6 years of age. This study had two primary aims. First, we aimed to describe patterns of early white matter development, including associations between tracts at each age and trajectories across time. Second, we aimed to predict individual differences in white matter microstructure at 6 years using values at earlier ages to determine at what point in development individual variability is established.

Materials and Methods

Subjects

Children in this study are part of the Early Brain Development Study, an ongoing longitudinal study at the University of North Carolina at Chapel Hill (UNC) (Knickmeyer et al. 2008, 2016; Gilmore et al. 2010). We have previously studied white matter development from birth to 2 years of age in this cohort (Geng et al. 2012; Lee et al. 2017; Girault et al. 2019), and we are now extending this study to ages 4 and 6 years. Parents were recruited from UNC hospitals during the second trimester of pregnancy, when they provided written informed consent. Subjects were included in the analyses for this study if they had valid DTI tract average data for at least one time point of data collection (neonate, 1, 2, 4, or 6 years of age; see Fig. 1). Exclusion criteria were premature birth (<37 weeks' gestation), over 24 h spent in the neonatal intensive care unit after birth, multiple gestation birth (e.g., twins), presence of a major medical event or MRI abnormality, diagnosis of a neurodevelopmental disorder by 6 years, or familial risk of psychiatric illness. If there were multiple children from the same family in the study, only one sibling's data were retained for data analysis. The sibling with the higher number of valid DTI acquisitions was kept in analysis, and if siblings had the same number of time points of DTI data, we prioritized the sibling with 6-year data. If both or neither had 6-year DTI data, one was randomly selected for inclusion.

Data were analyzed from 146 neonates, 91 one-year-olds, 62 two-year-olds, 84 four-year-olds, and 94 six-year-olds, across 224 unique subjects. Of these, over half (60.7%) had valid data for two or more DTI scans. Table 1 includes demographic data and scanning information for all subjects. Through age 2, subjects were scanned during natural sleep without sedation. At 4 and 6 years, children were given the option to watch a video during their scan. Scan success rates can be found in Table 2: the total number of children (after applying exclusion criteria) who were scanned, the number who provided at least some DTI data, and the number whose data were analyzed in this study.

Image Acquisition

All subjects were scanned using 3T scanners. Earlier DTI data were acquired on a 3T Siemens Allegra scanner (Siemens Medical Solutions), first obtaining six directions then updated to 42 directions. Later DTI data were acquired using a 3T Tim Trio. The change in scanner/sequence type resulted from the upgrades in MRI technology that occurred throughout the course of the longitudinal study. Refer to Table 1 for the distribution of subjects and scans across scanners. Supplementary Figure 1 illustrates the study timeline to clarify when the changes occurred and

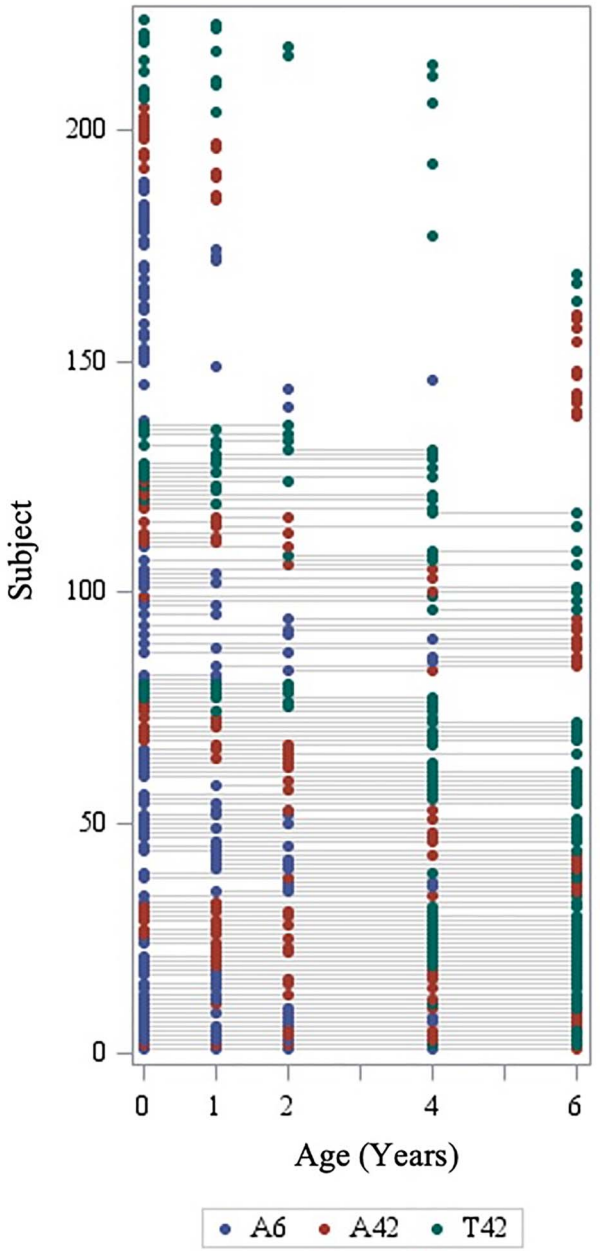

Figure 1. Overview of longitudinal sample, representing subjects with valid DTI tract average data at each age. A6, Allegra 6-direction DWI; A42, Allegra 42-direction DWI; T42, Trio 42-direction DWI.

how changes impacted the distribution of the sample across different scanners and sequence types. For the initial Allegra data, a single-shot echo-planar imaging spin-echo DTI sequence was used with the following parameters: TR/TE = 5200/73 ms, slice thickness = 2 mm, in-plane resolution = 2 × 2 mm^2, and a total of 45 slices. Each sequence acquired one baseline image ($b = 0$) and diffusion-weighted images along six gradient directions using a b value of 1000 s/mm^2. In order to improve signal-to-noise ratio (SNR), sequences were repeated five times and then combined into a single diffusion-weighted imaging (DWI) volume after motion correction. For the remaining Allegra data and all Trio data, 42 directions were acquired with a b value of 1000 s/mm^2 (in addition to 7 baseline images, $b = 0$), using the following parameters: TR/TE/Flip angle = 7680/82/90°, slice thickness = 2 mm, and in-plane resolution = 2 × 2 mm^2, with a total of 60–72 slices. It is noteworthy that with a single-shell acquisition, while we are able to estimate a good diffusion tensor model, this is insufficient for estimating or computing diffusion kurtosis (DKI; Steven et al. 2014) or more complex models such as neurite orientation dispersion and density imaging (NODDI; Zhang et al. 2012).

DTI Data Processing

A study-specific quality control protocol was applied to all raw DWI data using DTIPrep (www.nitrc.org/projects/dtiprep), which included slice-wise and gradient-wise artifact detection, as well as eddy current and motion correction (Oguz et al. 2014). This automatic quality control was followed by visual checking of all DWIs in order to exclude additional gradients containing artifacts not detected through the automatic processing. The number of excluded gradients through automatic and manual quality control checking provides a rough estimate of motion and image quality. Table 3 provides the average number of gradients excluded during both quality control steps. Images obtained using six directions had a maximum of 30 gradients, and 42-direction images had a maximum of 42 gradients. Neonate scans obtained with the six-direction protocol on the Allegra scanner had a significantly higher number of gradients excluded than did scans at all other ages using that scanner and protocol. In regard to the 42-direction protocol on both the Trio and Allegra scanners, 4- and 6-year-old scans had significantly more gradients excluded than scans at other ages.

DTI Atlas Mapping and Tractography

Skull and nonbrain tissue were masked out using the Brain Extraction Tool (BET; Smith 2002) on the average baseline ($b = 0$) image followed by manual mask corrections, if necessary. Tensors were estimated using a weighted least squares algorithm (Liu et al. 2010). Our fiber tract-based DTI processing pipeline included creating study-specific DTI atlases. Specifically, using the National Alliance for Medical Image Computing (NA-MIC) DTI fiber analysis framework (www.nitrc.org/projects/dtiatlas builder; Verde et al. 2014), we computed three age-specific atlases: an infant, a 1- to 2-year-old, and a 4- to 6-year-old DTI atlas. Deformation fields were computed to map each DTI scan into its corresponding atlas space. The 4- to 6-year-old DTI atlas was then deformable mapped into the 1- to 2-year-old DTI atlas space. For each 4- and 6-year scan, a single deformation field was computed by concatenating the two deformation fields (individual scan into atlas and 4- to 6-year atlas into 1- to 2-year atlas). The deformation fields were computed by matching intensity-normalized FA images and were then applied to the diffusion tensors; FA images were recomputed from the warped diffusion tensors. The atlas was then updated by computing it as the average over all warped tensors. Fiber tract segments were reconstructed in the neonate and 1- to 2-year atlases using streamline tractography using 3D Slicer (https://www.slicer.org). The same methodology was used to tract homologous fibers across both atlases, with identical, neuroanatomically guided seed targets identified in either native atlas space (see Supplementary Appendix of Lee et al. 2015). Visual inspection was done to ensure the fiber tracts appropriately reached the targets of interest, ensuring tracts are as similar as possible

Table 1 Participant demographic and scan information

	M (SD)			Range	
Gestational age, days	278.0 (7.6)			259–295	
Maternal education, years	16.3 (3.0)			8–25	
Birthweight, g	3470.1 (421.2)			2373–4701	
			N (%)		
Sex, male			110 (49.1%)		
Five scans			5 (2.2%)		
Four scans			27 (12.1%)		
Three scans			48 (21.4%)		
Two scans			56 (25.0%)		
One scan			88 (39.3%)		
	Neonate N = 146	1 Year N = 91	2 Years N = 62	4 Years N = 84	6 Years N = 94
	M (SD)	M (SD)	M (SD)	M (SD)	M (SD)
Age at scan (months)	0.69 (0.28)	12.67 (0.73)	24.62 (0.67)	49.17 (0.79)	73.75 (1.28)
	N (%)	N (%)	N (%)	N (%)	N (%)
Allegra, 6-direction	88 (60%)	38 (42%)	23 (37%)	9 (11%)	0 (0%)
Allegra, 42-direction	37 (25%)	32 (35%)	26 (42%)	20 (24%)	32 (34%)
Trio, 42-direction	21 (14%)	21 (23%)	13 (21%)	55 (65%)	62 (66%)

SD, standard deviation.

Table 2 Scan success rates by age

	Neonate N	1 Year N	2 Years N	4 Years N	6 Years N
MRI total	266	127	79	102	97
DWI total (% of MRI)	224 (84.2)	104 (81.9)	67 (84.8)	93 (91.2)	97 (100)
Tractography total (% of DWI total)	146 (65.2)	91 (87.5)	62 (92.5)	84 (90.3)	94 (96.9)

Note: MRI total is the number of children (after applying exclusion criteria) who provided at least some MRI data during the study visit. DWI total is the number of children who completed the DWI sequence during their visit. Tractography total is the number of children whose DWI scans passed each stage of quality control and tract profile generation.

Table 3 Summary of gradients excluded during automatic and visual quality control

	Neonate N = 146 M (SD) %	1 Year N = 91 M (SD) %	2 Years N = 62 M (SD) %	4 Years N = 84 M (SD) %	6 Years N = 94 M (SD) %
Allegra, 6-direction	4.93 (4.06)* 16%	1.50 (2.91) 5%	1.65 (3.30) 6%	2.33 (3.54) 8%	—
Allegra, 42-direction	5.10 (4.64) 12%	3.84 (3.26) 9%	3.62 (2.86) 9%	12.10 (5.10)* 29%	9.13 (5.04)* 22%
Trio, 42-direction	4.62 (5.11) 11%	5.43 (4.39) 13%	5.08 (3.04) 12%	11.95 (4.78)* 28%	7.95 (4.43)* 19%

Note: For the 6-direction scans, the maximum number of gradients is 30. For the 42-direction scans, the maximum number of gradients is 42.
*$P < 0.05$, values significantly larger than the other ages with the same scanner/sequence type.

across the two atlases. The infant and 1- to2-year-old DTI atlases as well as all fiber tracts employed in this work are publicly accessible as part of the UNC EBDS pediatric atlas distribution (https://www.nitrc.org/projects/uncebds_neodti/).

The following fibers, important for cognitive development, were included in this analysis: commissural bundles of the genu and splenium of the corpus callosum; projection fiber tracts of bilateral corticothalamic prefrontal projections (CTPF); association tracts of bilateral uncinate (UNC), bilateral inferior longitudinal fasciculus (ILF), bilateral superior longitudinal fasciculus (SLF), bilateral anterior cingulum (CGC), bilateral inferior fronto-occipital fasciculus (IFOF), and three bilateral segments of the arcuate fasciculus (ARC)—the direct (fronto-temporal) pathway (ARC-FT), the indirect anterior (fronto-parietal) pathway (ARC-FP), and the indirect posterior (temporo-parietal) pathway-ARC-TP). See Figure 2 for representations of these fiber bundles, which include nine left–right corresponding tracts and two commissural tracts. Fiber definitions have been described in

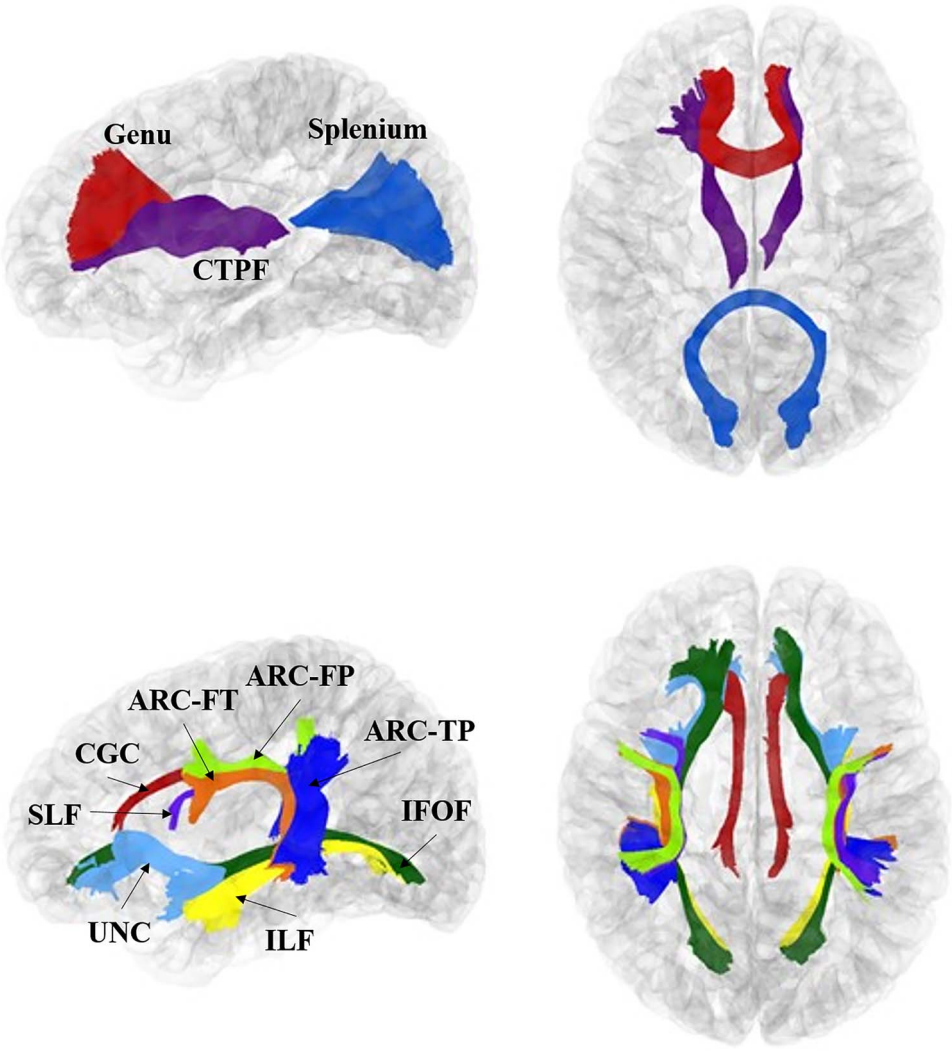

Figure 2. Tracts analyzed in the current study. These images were generated using 1-year cortical surfaces and tracts. Top: purple = corticothalamic prefrontal projections (CTPF); red = genu of corpus callosum (genu); blue = splenium of corpus callosum (splenium). Bottom: Light blue = uncinate (UNC); dark green = inferior fronto-occipital fasciculus (IFOF); yellow = inferior longitudinal fasciculus (ILF); red = cingulum (CGC); light green = arcuate fronto-parietal segment (ARCFP); orange = arcuate frontotemporal segment (ARCFT); blue = arcuate temporal-parietal segment (ARCTP); purple = SLF.

previous articles from our research group (Lee et al. 2015; Girault et al. 2019).

Diffusion property profiles were sampled along each fiber for axial diffusivity (AD), radial diffusivity (RD), and fractional anisotropy (FA). Profiles were thus sampled at equally spaced points along the length of each tract mapped back into each subject's original DTI space. Each tract from each scan underwent additional visual and quantitative diffusion profile quality control using FADTTSter (http://www.nitrc.org/projects/fadttster). Individual tracts were excluded if their FA profile had a correlation with the population average FA profile of <0.70. Some neonate tracts were reproduced less reliably across scans and therefore had higher failure rates than others (see Supplementary Table 1). Although for most tracts, very few subjects were excluded, there were three tracts that had higher levels of exclusions, all in neonates: ARCFP-R, ARCTP-L, and CGC-R. The arcuate tracts especially are difficult to track in infants due to the maturation and progression of myelination as well as crossing fibers (Dubois et al. 2016; Wilkinson et al. 2017). Additionally, terminal arc lengths for some tracts had high levels of noise and were accordingly cropped (Girault et al. 2019). In the neonate atlas, the following tracts were cropped: genu, IFOF-R, and UNC-R. In the 1- to 2-year and 4- to 6-year atlas, the following tracts were cropped: ILF-L and -R, CTPF-R, splenium, genu, ARC-TP-L and ARC-TP-R, and ARC-FT-L and ARC-FT-R. Overall average AD, RD, and FA values were computed for each tract, and these values were used in the analyses for this study.

Statistical Analysis

In addition to the tract quality control criteria described above, tract average value distributions were examined for outliers. If a value was more than three standard deviations from the mean, all three parameters generated from that subject's scan (at that age) were removed (see Supplementary Table 1). We examined tract averages for sex- and socio-economic status (SES)-based differences using bivariate correlations, considering

maternal education as a proxy for SES. We also plotted the mean AD, RD, and FA values for each scanner/sequence type, averaging across tracts for each age. An analysis of variance was used to test for differences between scanner/sequence types at each age for the three measures, with a Bonferroni correction applied to account for the three different measures across five different ages. We also examined tract asymmetries for pairs of left–right corresponding tracts by calculating lateralization values for AD, FA, and RD at each age, using the formula $\frac{L-R}{(L+R)/2}$, where L is the value for the left-hemisphere tract and R is the value for the right-hemisphere tract. A positive value for the lateralization measure indicates a higher tract average value of the left-hemisphere tract relative to the right-hemisphere tract. Left–right corresponding tracts were tested for asymmetries at each age using a paired t-test with a Bonferroni correction for all three measures across 5 years for the nine different bilateral tracts.

For each of the three DTI measures (AD, RD, or FA) at each of the 5 time points (neonate, 1, 2, 4, or 6 years), cross-sectional partial correlations between each of the 20 different tracts (9 left–right corresponding tracts and 2 commissural tracts) were calculated, including all individuals with valid data for each tract in a given year. Partial correlations control for child variables of age at MRI, sex, gestational age at birth, and birthweight, scanner/sequence type, and mother's education level. Correlations were then organized into a 20 by 20 correlation heatmap, with darker blue indicating a stronger positive correlation. For each of the partial correlations, a t-test after a Fisher z-transformation was used to test the null hypothesis that the true partial correlation is 0. In the heatmaps, all partial correlations that were not significant after a Bonferroni correction, accounting for all 190 pairwise correlations, were set to be 0 and therefore appear as white.

To illustrate tract-specific trajectories, the average of each of the three measures was calculated at each age and plotted with the average value on the y-axis and age on the x-axis. The average for a given tract for a given year was taken from all subjects with valid data for that tract at the given year. Using these values, we also calculated percent change between years. Additionally, to examine a different marker of tract maturity, we calculated the percent of 6-year FA values using FA of each tract at each previous age.

Linear models were used to obtain an estimate of how predictive DTI measures from earlier time points were the same for DTI measure at the final time point (6 years). For each DTI parameter for each tract, a model was fit using age at scan and scanner/sequence to predict the measure at each of the intermediate time points (neonate, 1, 2, and 4 years). The residuals from these models, which can be thought of as the DTI measures without the effect of age and scanner/sequence, were then used as a standardized version of the DTI measures in order to predict the same DTI measure in the same tract at year 6. Also included in each of the models were birthweight, gestational age at birth, sex, mother's education, age at 6-year scan, and scanner/sequence at 6-year scan. Individuals were included in the predictive models if they had valid data at the earlier time point, for all covariates, and at 6 years. The partial R^2 values for the DTI measure residuals from the earlier age represent how much variation in 6-year DTI measures can be explained by the same measures from an earlier age after controlling for all other covariates. Significance levels are also reported from an F-test of the null hypothesis that the true coefficient for the residuals of previous DTI measurement is zero in the model including all covariates. A Bonferroni correction for all three measures across 20 tracts and 4 ages was applied to these tests.

As a sensitivity analysis, we ran the same linear models using only subjects with the exact same scanner/sequence for year 6 and the same scanner/sequence at the intermediate time point. In order to ensure adequate sample size, we did not require this be the same scanner/sequence across all time points. In order to determine whether adding an earlier time point in addition to the 4-year measure would explain additional variance in 6-year measures, we ran an additional sensitivity analysis that included DTI measures at 6 years as the outcome and the same DTI measure residuals from year 4 as well as one of the other intermediate time points (neonate, 1 year or 2 years) as covariates. The same additional covariates as the other predictive models were also included. Further information on these analyses can be found with the supplementary tables.

Results

Descriptive Statistics

The tract average values included in the following analyses can be found in Supplementary Tables 2–4. All tract average values were first analyzed for differences based on sex or maternal education. Supplementary Tables 5–7 summarize the correlations between these demographic variables and tract average values. After Bonferroni correction for multiple comparisons, there is only one tract average value that had significant sex differences (4-year right cingulum AD) and one tract average value that is significantly associated with maternal education (2-year right cingulum AD) (see Supplementary Table 5). We also examined differences in tract average values across scanners and sequences (see Supplementary Fig. 2). The only age and parameter that significantly differs across scanner/sequence is AD at 1 year. Follow-up pairwise comparisons reveal that the AD values of images acquired with the Trio scanner using the 42-direction protocol are slightly (<3%) but significantly lower than those acquired using either of the Allegra sequences.

A number of pairs of left–right corresponding tracts show significant asymmetries after correction for multiple comparisons (see Supplementary Table 8). In general, tracts show the same lateralization pattern across ages and parameters, with almost every pair showing significant asymmetries in at least one parameter at each age. Notably, the ARC-FT has a different statistically significant asymmetry at birth (right FA is greater than left FA) than at later ages (left FA is greater). A similar pattern is shown with RD, though asymmetries at 4 and 6 are not statistically significant. Other tracts are consistent across ages: For example, UNC FA and AD are higher on the right, whereas ILF FA and AD are higher on the left.

Cross-Sectional Descriptions

The first aim of this study was to describe the characteristics of white matter tracts at different ages. Specifically, we conducted partial correlations across tracts to determine the extent to which microstructural properties were consistent across the brain at each age, controlling for child sex, gestational age at birth, birthweight, age at scan, scanner/sequence type, and maternal education. These correlations are displayed as heatmaps in Figures 3–5. Partial correlations between AD values across tracts become weaker over time: The average correlation

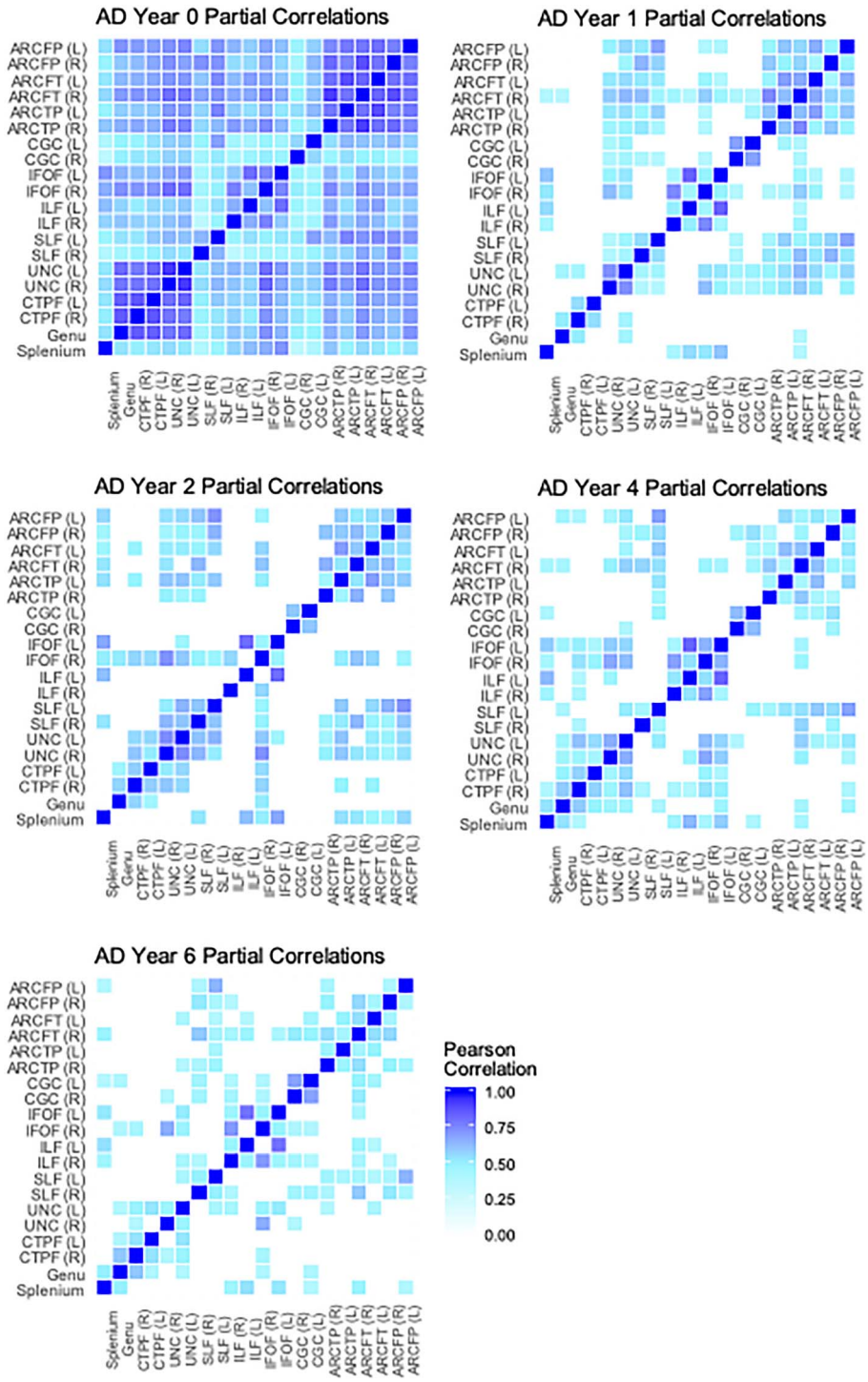

Figure 3. Cross-tract partial correlations of AD from birth through 6 years. Average partial correlations: neonate ($n = 146$) $M = 0.63$; 1 year ($n = 91$) $M = 0.36$; 2 year ($n = 62$) $M = 0.38$; 4 year ($n = 84$) $M = 0.36$; 6 year ($n = 94$) $M = 0.33$. White boxes represent nonsignificant partial correlations, after Bonferroni correction for multiple comparisons.

across tracts at birth is 0.63, but by 6 years the average has dropped to 0.33 (see Fig. 3). Average correlations for RD at birth are relatively stronger than at later ages (0.78 vs. between 0.63 and 0.67), though there does not appear to be as much change across ages for FA. Generally, the highest correlations are found between corresponding tracts in opposite hemispheres (e.g., left and right cingulum). Additionally, a few other tracts are relatively highly correlated across ages and parameters: for example, between the IFOF and the ILF, the IFOF and the UNC, and among the different arcuate (ARC) segments.

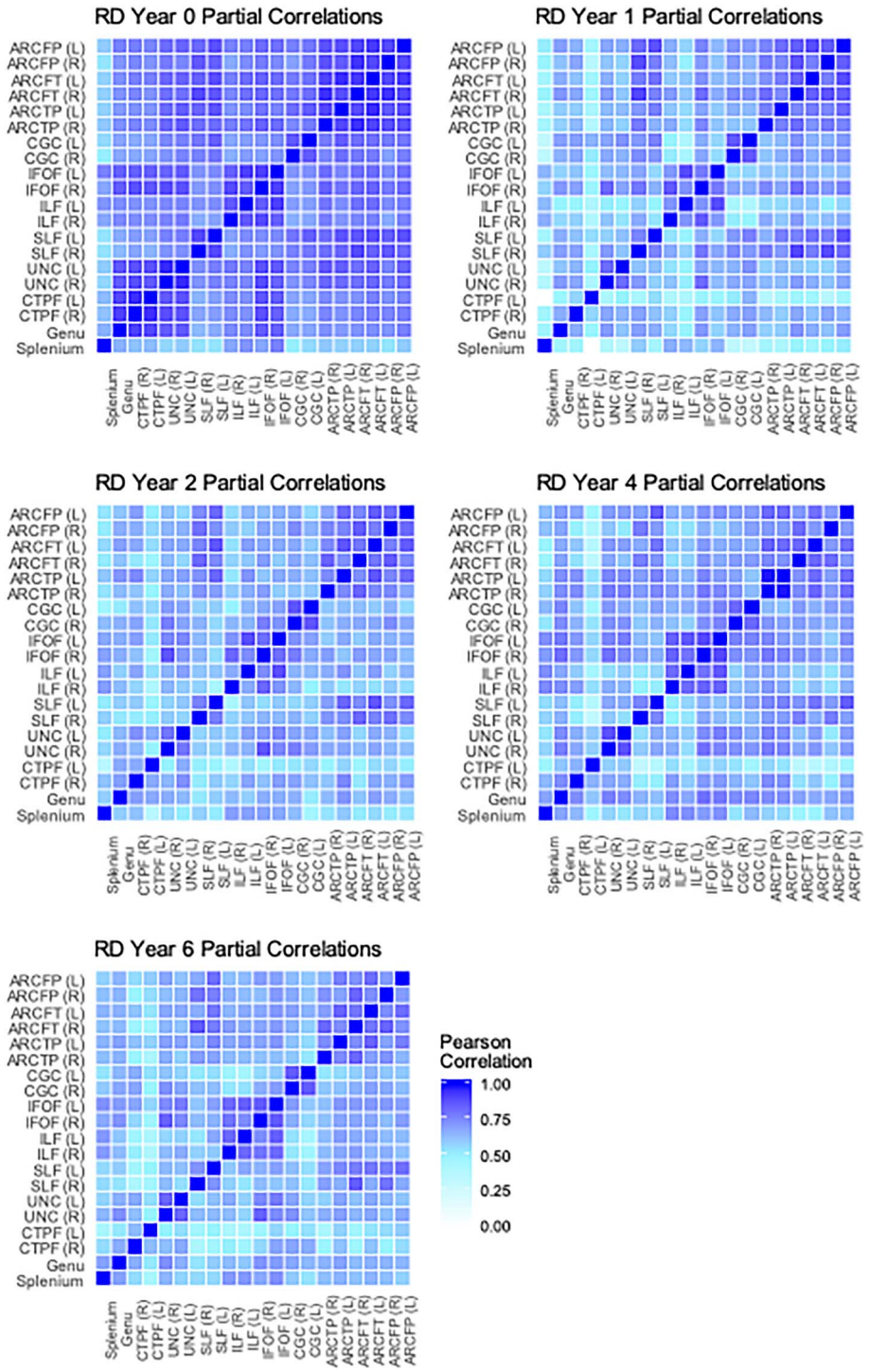

Figure 4. Cross-tract partial correlations of RD from birth through 6 years. Average partial correlations: neonate ($n = 146$) $M = 0.78$; 1 year ($n = 91$) $M = 0.63$; 2 years ($n = 62$) $M = 0.65$; 4 years ($n = 84$) $M = 0.67$; 6 years ($n = 94$) $M = 0.64$. White boxes represent nonsignificant partial correlations, after Bonferroni correction for multiple comparisons.

Tract Trajectories

Our next aim was to visualize the trajectories of white matter microstructural development from birth through 6 years. These trajectories can be found in Figure 6 and represent the mean tract average values for each parameter across age. The values represented in these plots are presented in Supplementary Tables 2–4. As expected, both AD and RD decrease over time, and FA increases over time. For all three parameters, the most rapid change occurs between birth and 1 year, though this change is more pronounced in RD and FA than in AD. Considering average AD and FA, tracts generally maintain rank order, such that those with relatively higher values at birth

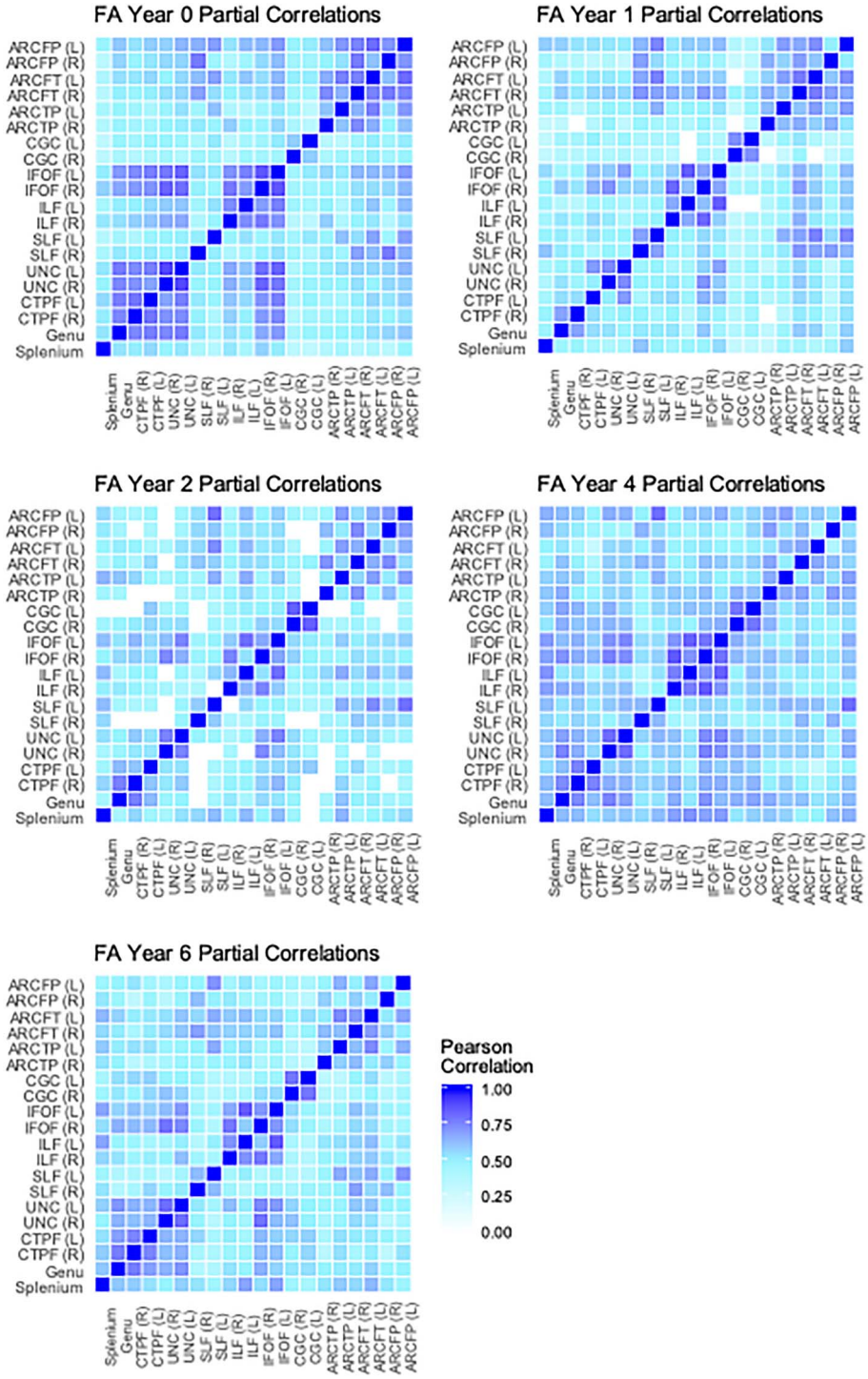

Figure 5. Cross-tract partial correlations of FA from birth through 6 years. Average partial correlations: neonate ($n = 146$) $M = 0.56$; 1 year ($n = 91$) $M = 0.51$; 2 year ($n = 62$) $M = 0.51$; 4 year ($n = 84$) $M = 0.59$; 6 year ($n = 94$) $M = 0.53$. White boxes represent nonsignificant partial correlations, after Bonferroni correction for multiple comparisons.

remain higher across time. Rank order of tracts by RD values is less consistent from birth to 1 year but appears to stabilize from 1 to 6 years.

Using the mean tract average values across all tracts at each age, we estimated the percent change between years (see Table 4). Between the neonate and 1-year scans, there is a 71.3% increase in average FA, along with a 13.7% decrease in average AD and a 32.2% decrease in average RD. These changes are substantially greater than the microstructural changes in subsequent years (represented by increases in FA and decreases in AD and RD). Each of these findings confirms the patterns seen in the tract average trajectories.

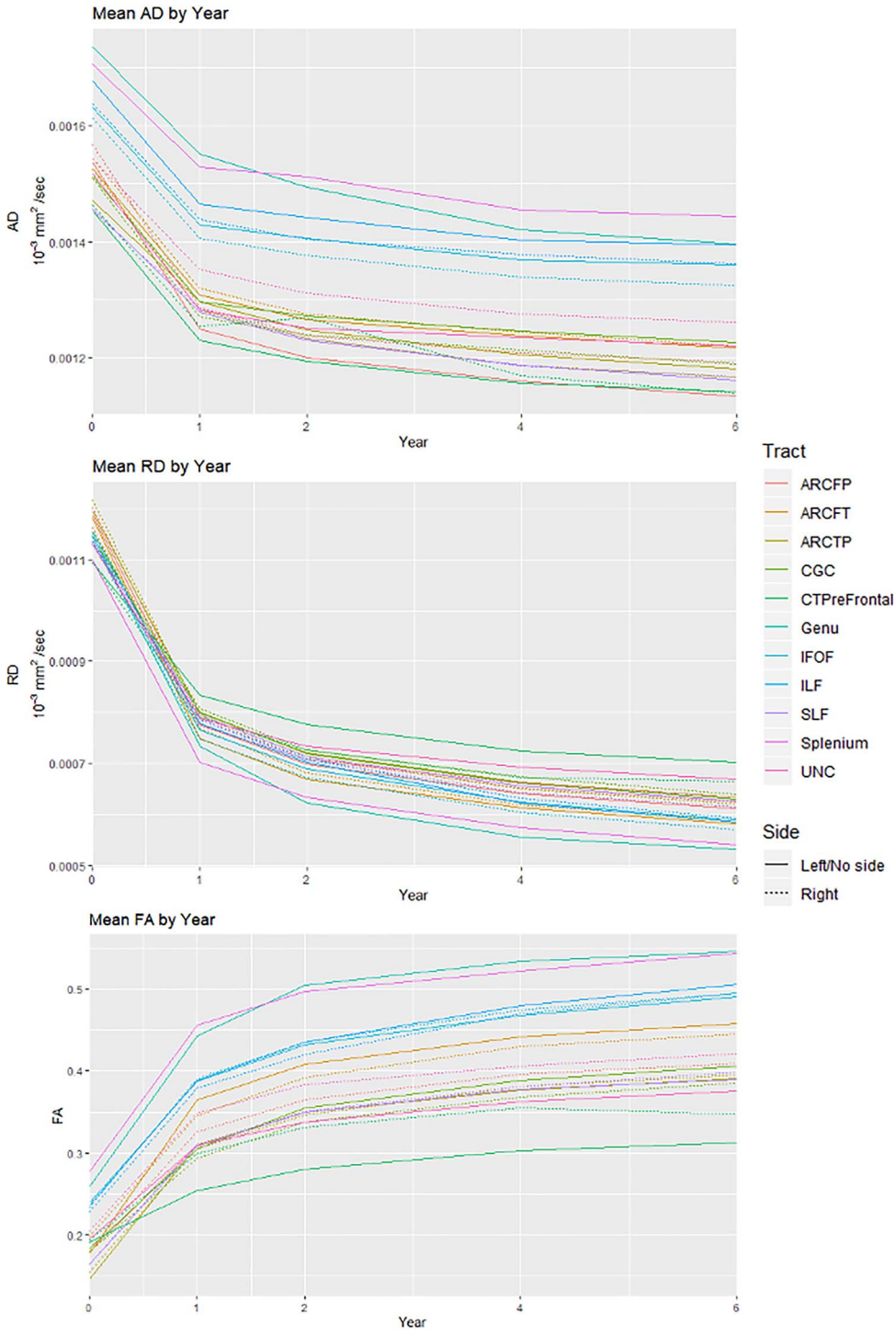

Figure 6. Trajectories of AD, RD, and FA from birth through 6 years.

We also considered FA values at each age as a proportion of 6-year FA for each tract. These values are presented in Figure 7. There are some notable patterns in these results. For example, the CTPF tracts are relatively closer to their 6-year FA values at birth, as compared with other tracts. The ARC segments, on the other hand, are relatively lower proportions of 6-year FA at birth, with these proportions all below the average. There was a much larger range for the neonate proportions of 6-year FA (0.37–0.60) as compared with 1-year (0.74–0.86), 2-year (0.84–0.94), and 4-year (0.93–1.02) proportions.

Individual Differences

The second aim of this study was to understand when in development individual differences in white matter microstructure arise by measuring the predictive value of each microstructural

Table 4 Average AD, RD, and FA values and percent changes across ages

	AD (10^{-3} mm^2/s) M (SD)	RD (10^{-3} mm^2/s) M (SD)	FA M (SD)
Neonate average	0.00155 (2.9e−4)	0.00115 (2.8e−4)	0.200 (0.08)
1-Year average	0.00134 (1.9e−4)	0.00078 (1.5e−4)	0.342 (0.09)
2-Year average	0.00131 (1.9e−4)	0.00070 (1.4e−4)	0.383 (0.09)
4-Year average	0.00126 (1.8e−4)	0.00064 (1.5e−4)	0.415 (0.12)
6-Year average	0.00125 (1.6e−4)	0.00061 (1.4e−4)	0.430 (0.11)
	%	%	%
% Change neo-1	13.7	32.2	71.3
% Change 1–2	2.7	9.9	12.1
% Change 2–4	3.1	8.5	8.3
% Change 4–6	1.5	4.6	3.7
% Change neo-6	19.9	46.7	115.5
% Change 1–6	7.1	21.4	25.8

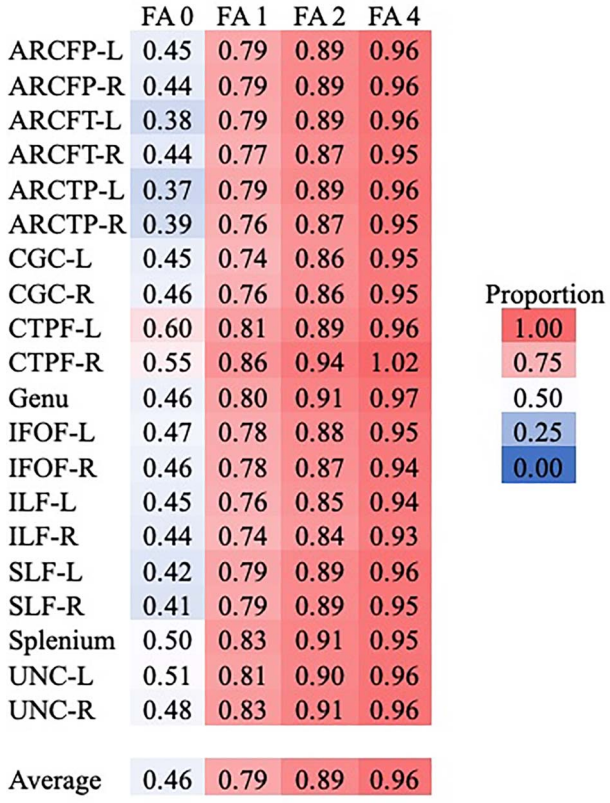

Figure 7. Heatmap of the proportion of 6-year FA values by each tract at earlier ages.

property at each age for the respective property at 6 years. This was done by fitting regression models to predict the 6-year tract average from the respective standardized parameter at each earlier age. Partial R^2 values for these models can be found in Figure 8, with model P values in Supplementary Table 9. All models included covariates of child sex, birthweight, gestational age at birth, maternal education, child's age at 6-year scan, and the scanner/sequence type for the 6-year scan. These models only included the subset of subjects with tract average data at 6 years and at least one previous scan (neonate, 1, 2, or 4 years). Sample sizes for these models can be found in Figure 8.

Overall, individual differences in AD, RD, and FA at 6 years are weakly explained by variability in these parameters at birth (on average, 9–16%), with very few parameter estimates reaching statistical significance. The average predictive value of tract microstructure at 1 year is much stronger: 31% for AD, 44% for RD, and 52% for FA. Generally, AD at 1 year is slightly less predictive of 6-year AD, compared with the predictive values of RD and FA, except in IFOF and ILF tracts. The predictive values of these parameters continue to increase with age; the models predicting 6-year tract average values from respective 4-year values are the strongest, with tract average values uniquely explaining on average more than 50% of the variance in respective 6-year parameters. Even after Bonferroni correction (the most conservative type of correction), the majority of models predicting 6-year values from 1-, 2-, and 4-year tract average values remain significant (see Fig. 8).

Although these models suggest that 4-year microstructural parameters explain a significant amount of variance in 6-year values, more so than earlier ages, we ran a series of follow-up analyses that included earlier ages in addition to the 4-year time point. Adjusted R^2 for these models can be found in Supplementary Tables 10–12. For the vast majority of these models, adding an earlier time point did not contribute above and beyond what could be explained by the 4-year parameter alone. Additionally, these models include much smaller subsamples, as each requires that an individual child has valid data for three scans (4-year, 6-year, and the earlier time point).

As scanner heterogeneity is a complicating factor, even when controlling for scanner/sequence, we ran similar regression models in subsets of children who were all scanned using one protocol (e.g., 6-direction Allegra) at the earlier time point and one protocol (e.g., 42-direction Trio) at the 6-year scan, selecting the scanner/sequence combination with the largest sample size. (There were no children who were scanned with the same protocol at every age.) Supplementary Table 13 summarizes these results. Because these models utilize only a subset of scores, model sample sizes are much smaller (range $n = 16$ to $n = 34$). However, average partial R^2 values are largely similar to those values obtained in the full models (Fig. 8). The main

	AD				RD				FA			
	neo	1yr	2yr	4yr	neo	1yr	2yr	4yr	neo	1yr	2yr	4yr
ARCFP-L	.03	.33	.20	**.49**	.16	**.47**	.32	**.56**	.06	**.53**	**.62**	**.74**
ARCFP-R	.16	.09	.21	**.46**	.05	**.43**	**.58**	**.46**	.00	**.44**	**.55**	**.62**
ARCFT-L	.05	.23	.39	**.39**	.21	**.49**	**.73**	**.61**	.21	**.61**	**.81**	**.74**
ARCFT-R	.10	.33	.44	**.34**	.19	**.51**	**.65**	**.51**	.16	**.54**	**.58**	**.60**
ARCTP-L	.02	.31	**.48**	**.46**	.09	**.39**	**.64**	**.63**	.01	**.62**	**.66**	**.65**
ARCTP-R	.03	.12	**.65**	**.50**	.23	**.52**	**.68**	**.42**	.15	**.35**	.47	**.58**
CGC-L	.03	**.36**	.44	**.38**	.19	**.36**	.28	**.44**	.14	**.63**	**.50**	**.48**
CGC-R	.01	**.41**	.43	**.39**	**.32**	**.45**	**.59**	**.45**	.21	**.60**	**.64**	**.50**
CTPF-L	.03	.30	**.60**	**.54**	.12	.35	**.70**	**.75**	.25	**.45**	.35	**.65**
CTPF-R	.10	**.44**	**.46**	**.62**	.11	**.53**	**.65**	**.54**	.20	**.54**	.40	**.41**
Genu	.02	.26	.28	**.39**	.15	**.40**	**.49**	**.43**	.21	**.49**	**.48**	**.54**
IFOF-L	.25	**.50**	**.60**	**.68**	.24	**.52**	**.59**	**.68**	.18	**.59**	**.63**	**.70**
IFOF-R	.11	**.38**	.35	**.54**	.21	**.46**	.19	**.53**	.11	**.44**	.12	**.55**
ILF-L	.27	**.54**	**.72**	**.80**	.24	**.54**	**.63**	**.67**	**.29**	**.58**	**.67**	**.65**
ILF-R	.15	**.53**	**.48**	**.62**	.18	**.55**	.44	**.64**	.11	**.54**	.20	**.48**
SLF-L	.09	.16	.43	**.37**	.14	**.40**	**.63**	**.56**	.04	**.42**	**.61**	**.64**
SLF-R	.15	.20	.43	**.54**	.00	**.57**	**.59**	**.73**	.19	**.68**	.33	**.77**
Splenium	.15	.15	.28	**.51**	.07	.28	**.45**	**.67**	.00	**.35**	.43	**.58**
UNC-L	.07	.31	.26	**.48**	.18	**.40**	**.51**	**.59**	.07	**.55**	**.53**	**.57**
UNC-R	.04	.30	**.56**	**.40**	.20	**.55**	.43	**.63**	.10	**.64**	**.57**	**.61**
Average	.09	.31	.43	.50	.16	.46	.54	.57	.14	.53	.51	.60

Figure 8. Heatmap representing partial R^2 values for individual tracts predicting 6-year tract averages. Values in bold represent models with coefficients that were statistically significant after Bonferroni correction for multiple comparisons. *P* values for the tract average coefficients in these models can be found in Supplementary Table 2. Model sample sizes: neonate to 6 years, $n = 50$; 1–6 years, $n = 42$; 2–6 years, $n = 32$; 4–6 years, $n = 53$.

exception was the models predicting 6-year RD from 2-year RD. Given that this is the only parameter and predictor age that differed greatly, we attribute these differences to the small subset sample size, which is only half that of the full model sample.

Discussion

To our knowledge, this is the first study to follow a sample of children from birth through 6 years, allowing for within-subject analyses of longitudinal data. The most notable finding from these analyses is that a large portion of variance in 6-year tract microstructure can largely be explained by microstructure at 1 year, especially as reflected in RD and FA. By 1 year, tract averages are largely significantly predictive of their respective 6-year values, accounting for, on average, 40% or more of the variance in microstructural parameters. By contrast, only about 10% of the variance in 6-year values could be accounted for by the tract average values at birth. This suggests that white matter microstructure at 1 year of age may be helpful for predicting later tract characteristics or potentially other outcomes. With age, there are incremental improvements in predictive value, as expected, but the largest increase occurs between birth and 1 year. Our results suggest that individual differences in RD, which is thought to reflect myelination in the developing brain, are more established by age 1 than are individual differences in AD, which is thought to reflect fiber organization and density (Dubois et al. 2014). However, it is interesting that AD values at 1 year for both left and right IFOF and ILF were significantly predictive of 6-year values, suggesting that these tracts are relatively more organized at 1 year compared with other tracts.

Cross-sectional correlations suggest that at birth, microstructural patterns are fairly consistent across tracts. Across all three parameters, cross-tract correlations were stronger at birth than at subsequent ages. Decreases in cross-tract correlations may reflect different levels of maturity between tracts that occurs as some networks mature earlier and more quickly than others. Previous research has established conflicting patterns of correlations across tracts. For example, in a larger sample (one that included twin pairs), our research group found similar results to the current study, with correlations decreasing between birth and 2 years (Lee et al. 2017). On the other hand, Mishra et al. (2013) found that intertract correlations became stronger between birth and puberty, though this was in a small cross-sectional sample. The differences between studies are likely due to maturational changes between 6 years and

adolescence; however to our knowledge, no existing research has directly explored this pattern.

Although the general strength of partial correlations between tracts across time differs across parameters, when looking at pairs of tracts with higher correlations, some distinct patterns emerge. The pairs of tracts with relatively high partial correlations across ages and parameters were corresponding tracts in opposite hemispheres or those that are generally anatomically proximate or connecting nearby cortical areas. For example, we see strong partial correlations between the IFOF and the ILF, as well as between different ARC segments. Tracts that are in similar anatomical locations within the brain are likely to exhibit similar patterns in microstructural development, since it is well known that myelination and white matter maturation occurs in a particular spatial pattern. Additionally, it is possible that the tracts with high correlations may track through some of the same voxels.

The plots illustrating the changes in tract averages from birth to 6 years are largely consistent with previous research on early white matter development (Dubois et al. 2014). As expected, AD and RD decreased while FA increased across age. The most rapid changes across all three parameters occur between birth and 1 year. In fact, the changes in parameter values in this first year alone are substantially greater than the additional changes that occur between 1 and 6 years, as summarized in Table 3, though the average change in AD from birth to 1 year is smaller than the changes in RD and FA in that same timeframe. Additional research suggests that microstructural changes after 6 years, though not insignificant, are relatively small compared with the development observed during infancy and early childhood (Lebel and Beaulieu 2011; Lebel et al. 2019). The patterns established in this study, in conjunction with research on older children and adults, confirm that the first year is especially important for establishing the foundation for later white matter development.

The proportion of 6-year FA accounted for by earlier ages further supports the claim about the importance of the first year of life. There is a much greater range of proportions at the neonate scan than for any of the subsequent scans. These analyses also suggest that the CTPF tracts are more similar to their 6-year FA values at birth compared with other tract proportions. Although we would expect tracts that project to the prefrontal cortex to mature later, corticothalamic tracts are among the earliest to mature. The arcuate segments, on the other hand, show relatively lower proportions of 6-year FA at birth, compared with the other tracts.

Results from our analysis of tract asymmetries are interesting, considering the role of the arcuate in early language development. The frontotemporal segment of the arcuate fasciculus (ARC-FT) showed a different asymmetry pattern across the first 6 years than any other pair of corresponding tracts. Specifically, at birth, the right ARC-FT had higher FA and lower RD, but at 1 year and later, the left ARC-FT had higher FA and lower RD. Given the well-established leftward asymmetry of the arcuate and the role of the left ARC-FT in language development in adults and children (e.g., Catani et al. 2005; Lebel and Beaulieu 2009), it stands to reason that exposure to language input during the first few years would result in differential maturation of the corresponding segments. However, we recommend caution in interpreting these asymmetry results as left and right bundles were not symmetric in the atlases. Additionally, cropping was applied based on noise levels at the end of tracts, without any attempt to ensure symmetrical cropping across left–right corresponding tracts.

Our results suggest that microstructural properties, namely, FA and RD, in a subset of fibers at age 1 explain significant variation in those same metrics 5 years later at age 6. These findings echo a body of work reporting that white matter properties measured by diffusion MRI undergo substantial development in the first year of life (Geng et al. 2012; Dubois et al. 2014; Girault et al. 2019), with measurable myelin content in the brain increasing rapidly in the latter part of the first year (Deoni et al. 2011). The lack of association between WM metrics at birth and age 6 is most likely explained by the dramatic developmental growth that occurs during this first postnatal year, which may be driven to a greater extent by perinatal and environmental factors than at later ages. Twin studies support this hypothesis by demonstrating that the heritability of white matter integrity increases from birth to ages 1 and 2 (Lee et al. 2015; Lee et al. 2019), suggesting that environmental factors (or measurement error) accounts for more variability in white matter microstructure at birth than later ages.

Generally stronger associations across development for FA and RD compared with AD, as indicated by both the partial correlation heatmaps and the predictive models, may be due to the lack of biological specificity reflected in AD as it relates to myelination (Dubois et al. 2014). The partial correlations across tracts using AD are notably weaker at ages 1 year and older, compared with those correlations using RD and FA, as shown by the number of boxes in each heatmap indicating nonsignificant partial correlations. We also observed the least amount of change in tract averages of AD across development compared with RD and FA. For AD, fewer tracts at 1 and 2 years have significant associations with values at 6 years compared with RD, for which most tracts at 1 year are significantly predictive of 6-year values. AD is thought to be a marker of axonal organization and integrity, while RD tracks more consistently with premyelination and myelination (Dubois et al. 2014). Thus, the relatively small change in AD over time may reflect the inherent organization of the axonal network, which is established in utero and primarily modified postnatally through myelination (Ball et al. 2014; Dubois et al. 2014). Overall our results suggest that individual differences in the processes that RD represents, including myelination, are present earlier in development than those that AD represents. However, we suggest caution in the interpretation of the specific biological mechanisms underlying developmental changes diffusion parameters, as most of what we know about specific mechanisms of AD, RD, and FA come from rodent studies of axonal injury and dysmyelination or simulations (Winklewski et al. 2018), not typical development.

Previous research describes different rates of development for association, projection, and commissural tracts (e.g., Lebel and Beaulieu 2011; Geng et al. 2012; Dubois et al. 2014; Lee et al. 2017). Our results demonstrate some consistency with this categorization. For example, the two commissural tracts analyzed in the current study, the genu and splenium, have the highest FA values across age (see Fig. 6 and Supplementary Table 5). Additionally, splenium FA at birth is a relatively high proportion of FA at 6 years, relative to many of the other tracts. Tracts, with the strongest associations with 6-year microstructure implicated across multiple diffusion parameters and developmental time points (Fig. 8), were primarily association fibers, including segments of the ARC, IFOF, ILF, SLF, and UNC. These tracts provide pivotal connections between the frontal and temporal

(ARC, UNC), frontal and parietal (ARC, SLF), parietal and temporal (ARC), visual and temporal (ILF), and visual and frontal (IFOF). Many of these fibers run parallel to each other and exhibit coordinated development (Figs 3–5), especially the IFOF and ILF, and segments of the ARC. The strong developmental associations between maturational properties of these tracts between the first and sixth year of life suggest these tracts are structurally defined early in development and thus may be important for subsequent cognition and learning. In fact, each of these tracts has been shown to relate to emerging cognition in the first 2 years of life in an overlapping sample (Girault et al. 2019), with developmental changes in RD in each of these tracts in the second year of life linked to receptive language outcomes at age 2 (Girault et al. 2019). Taken together, this work highlights that microstructural properties of these tracts in early postnatal development carry important information for proximal cognition in toddlerhood and distal white matter integrity. Additional work has demonstrated associations between such cognitive abilities in toddlerhood and aspects of executive function and intelligence in early childhood (Girault et al. 2018; Stephens et al. 2018). Therefore, white matter integrity in the early years may serve as an important biomarker of subsequent outcomes. Future work should seek to identify longitudinal associations between white matter properties in these tracts and cognitive and behavioral outcomes in later childhood.

Results from both the predictive models and from the comparisons of tract average values across ages suggest that individual differences in white matter microstructure are more or less stable by 1 year of age. This pattern is similar to what has been established for gray matter volume (Knickmeyer et al. 2008; Gilmore et al. 2012). These findings are also in line with results from longitudinal intervention research that describes early sensitive periods in development. For example, aspects of nurturing and sensitive caregiving are especially important during the first year of life (Nelson et al. 2007; Fox et al. 2011). Additionally, analysis of resting state connectivity patterns during the first year of life reveals that primary networks, those that serve auditory, sensory, and motoric functions, take form and resemble adult-like networks by 12 months of age (Gao et al. 2015). Similarly, in terms of behavior, infants' ability to discriminate auditory (i.e., phonemes) and visual stimuli (i.e., faces of other species) narrows in terms of sensitivity and accuracy, becoming adult-like by the end of the first year of life (Werker and Tees 1984; Pascalis et al. 2002; Best and McRoberts 2003; Kuhl et al. 2006). Each of these areas of research provides additional support for the importance of the first year of life as foundational for long-term neurological and behavioral outcomes.

One tract that was not included in the results presented in this manuscript is the fornix, an association tract that has been tied to a number of behavioral and psychiatric outcomes (Tsivilis et al. 2008; Fitzsimmons et al. 2009; Wolff et al. 2012; Douet and Chang 2015). Although a tract profile for the fornix was generated using the tractography methods described, initial exploration of the fornix tract average values revealed outlying values and inconsistent patterns. As a result, we do not consider the fornix values generated by these methods to be valid and have therefore not included the findings related to this tract in this manuscript. Other studies have reported similar data processing concerns with the fornix and have attributed this to the tract's tubular shape and its location in regard to subcortical structures (Acheson et al. 2017; Pecheva et al. 2017). Additional white matter tracts may have also been considered (e.g., corticothalamic projections to areas of the cortex other than prefrontal regions). In order to limit the number of analyses in this study, we opted to focus on tracts that have been linked to various aspects of cognition. We therefore are not presenting an exhaustive view of white matter maturation; we have chosen to provide an overview of development within a set of relevant tracts. Future research should examine patterns of development and individual differences in tracts that have been tied to other aspects of development, such as other projection tracts, especially those that are known to mature at different ages.

The use of DTI parameters to assess white matter microstructure has a number of limitations. First, while we have some knowledge of how diffusion metrics change across development, and how they relate to primary processes such as fiber organization, premyelination, and myelination, we cannot rule out the contribution of other confounding factors—including crossing fibers, the myelination of crossing fibers, and partial volume effects—on tensor estimation (Vos et al. 2011; Dubois et al. 2014). More recently developed methods including NODDI (Zhang et al. 2012) and diffusion kurtosis imaging (DTK; Steven et al. 2014) offer improved algorithms for estimating local diffusion patterns that better reflect the underlying biology and physiology of white matter. However, NODDI and DTK require DWI sequences that were not standard at the start of this longitudinal imaging study in 2004. Future studies using these advanced sequences will be needed to further clarify our understanding of white matter development in the human brain.

A limitation of the current study is that almost 40% of the sample analyzed only provided data at one time point. This is due to sample attrition as well as exclusions due to image quality. Another potential limitation to this study is the use of a separate atlas for the neonate data. The decision to not also map the neonate atlas to the 1- to 2-year-old atlas (as we did with the 4- to 6-year-old atlas) was based on differences in the shape and size of the neonate brain. Fitting the neonate white matter tracts to the pediatric atlas would likely result in distortions that cause inaccuracies in the tract average values calculated. Therefore, we determined that the neonate atlas generated more accurate representations of the tracts.

Another limitation is the aggregation of data from multiple scanners and different DTI acquisition protocols. This concern is an inherent limitation of longitudinal research, especially in regard to adapting to advances in MRI technology. However, across ages and parameters, only average 1-year AD significantly differed across scanners/sequences. We have made every effort to reduce potential influences of these differences by including the scanner type and number of directions in predictive models. In future studies that utilize data from different scanners and sequences, we will consider the use of data harmonization methods such as ComBat (Fortin et al. 2017). Relatively, lack of predictive ability at the neonate time point may be partially due to higher levels of noise and more gradients excluded on average. The FA images for neonates have lower SNR due to less myelination throughout the brain, and more of this age group was scanned using the 6-direction protocol, which also has a lower SNR. As a result, minor motion is more likely to lead to rejection based on image quality. Lastly, the predictive models only include a subset of subjects who provided valid data at both 6 years and at least one earlier time point, resulting in relatively small sample sizes and models using different combinations of subjects. Though most of the models are statistically significant

(even after correction for multiple comparisons) despite the smaller subsamples, models lack the power to make strong claims especially regarding tract-level differences.

Our research group is continuing to follow this longitudinal sample with the ultimate goal of being able to track white matter development from birth through early adolescence. Additional research should continue to explore brain development in such longitudinal samples in order to gain a better understanding of individual differences over time. Further, we have limited these analyses to tract averages, so future research should examine regional differences and patterns of development, as well as whole-brain approaches to white matter maturation (i.e., TBSS; Smith et al. 2006). The methods employed in this study should also be extended to less normative samples to determine how patterns of development may differ in children who were born premature, who are at high risk for psychiatric disorders, or in twin samples. Further, steps should be taken to examine how individual patterns of development relate to cognitive, behavioral, or psychiatric outcomes. Bivariate correlations between microstructural parameters and demographic variables of sex and maternal education suggest a potentially interesting association with right cingulum AD. Further exploration of this association is warranted. Although there is value in exploring how white matter relates to these outcomes cross-sectionally, longitudinal study designs will provide greater opportunities for identifying early biomarkers that are related to a range of later outcomes. Such research could then lead to additional explorations of sensitive periods of development and the ideal timing of early intervention programs.

This study provides unique insight into patterns of early white matter development by connecting two previously disparate bodies of research (i.e., the first 2 years vs. early childhood through adulthood) and by exploring development in a truly longitudinal sample of children (most previous research can more accurately be described as cohort-sequential). Consistent with previous research, white matter maturation during the first year is much more prolific and occurs at a faster rate than during subsequent years. Although our results suggest that white matter microstructure at birth may not be helpful in terms of identifying early biomarkers predictive of later white matter development, by 1 year of age, individual differences as well as overall group averages are much more consistent with 6-year microstructure across tracts. This rapid development during the first year, as guided by biological maturation and environmental influences, sets the foundation for continued development.

Notes

The authors thank the participating families, the researchers at the UNC NeuroImage Research and Analysis Laboratories, and the study coordinators of the UNC Early Brain Development Study. The views expressed in this manuscript are those of the authors and do not necessarily represent the opinions or position of listed funding agencies.

Conflict of Interest: None declared.

Funding

National Institutes of Health (grant numbers HD053000, MH064065, MH070890, and MH111944 to J.H.G); National Institute of Mental Health (grant numbers T32-MH106440 to R.L.S. and B.W.L., MH099411 to S.J.S.); National Institute of Child Health and Human Development (grant numbers T32-HD007376 and T32-HD40127 to J.B.G.).

References

Acheson A, Wijtenburg SA, Rowland LM, Winkler A, Mathias CW, Hong LE, Jahanshad N, Patel B, Thompson PM, McGuire SA *et al*. 2017. Reproducibility of tract-based white matter microstructural measures using the ENIGMA-DTI protocol. *Brain Behav.* 7:e00615.

Ball G, Aljabar P, Zebari S, Tusor N, Arichi T, Merchant N, Robinson EC, Ogundipe E, Rueckert D, Edwards AD *et al*. 2014. Rich-club organization of the newborn human brain. *Proc Natl Acad Sci. U S A* 111:7456–7461.

Best CC, McRoberts GW. 2003. Infant perception of non-native consonant contrasts that adults assimilate in different ways. *Lang Speech*. 46:183–216.

Catani M, Jones DK, ffytch DH. 2005. Perisylvian language networks of the human brain. *Ann Neurol*. 57:8–16.

Deoni SCL, Dean DC, O'Muircheartaigh J, Dirks H, Jerskey BA. 2012. Investigating white matter development in infancy and early childhood using myelin water faction and relaxation time mapping. *Neuroimage*. 63:1038–1053.

Deoni SCL, Mercure E, Blasi A, Gasston D, Thomson A, Johnson M, Williams SCR, Murphy DGM. 2011. Mapping infant brain myelination with magnetic resonance imaging. *J Neurosci*. 31:784–791.

Douet V, Chang L. 2015. Fornix as an imaging marker for episodic memory deficits in healthy aging and in various neurological disorders. *Front Aging Neurosci*. 7:1–19.

Dubois J, Dehaene-Lambertz G, Kulikova S, Poupon C, Hüppi PS, Hertz-Pannier L, Sehaene-Lamberts G, Kulikova S, Poupon C, Huppi PS *et al*. 2014. The early development of brain white matter: a review of imaging studies in fetuses, newborns and infants. *Neuroscience*. 276:48–71.

Dubois J, Poupon C, Thirion B, Simonnet H, Kulikova S, Leroy F, Hertz-Pannier L, Dehaene-Lambertz G. 2016. Exploring the early organization and maturation of linguistic pathways in the human infant brain. *Cereb Cortex*. 26:2283–2298.

Feldman HM, Yeatman JD, Lee ES, Barde LHF, Gaman-Bean S. 2010. Diffusion tensor imaging: a review for pediatric researchers and clinicians. *J Dev Behav Pediatr*. 31: 346–356.

Fields RD. 2008. White matter in learning, cognition and psychiatric disorders. *Trends Neurosci*. 31:361–370.

Filley CM, Fields RD. 2016. White matter and cognition: making the connection. *J Neurophysiol*. 116:2093–2104.

Fitzsimmons J, Kubicki M, Smith K, Bushell G, Estepar RSJ, Westin CF, Nestor PG, Niznikiewicz MA, Kikinis R, McCarley RW *et al*. 2009. Diffusion tractography of the fornix in schizophrenia. *Schizophr Res*. 107:39–46.

Fortin JP, Parker D, Tunc B, Watanabe T, Elliott MA, Ruparel K, Roalf DF, Satterthwaite TD, Gur RC, Gur RE *et al*. 2017. Harmonization of multi-site diffusion tensor imaging data. *Neuroimage*. 161:149–170.

Fox SE, Levitt P, Nelson CA III. 2011. How the timing and quality of early experiences influence the development of brain architecture. *Child Dev*. 81:2011.

Gao W, Alcauter S, Smith JK, Gilmore JH, Lin W. 2015. Development of human brain cortical network architecture during infancy. *Brain Struct Funct*. 220:1173–1186.

Gao W, Lin W, Chen Y, Gerig G, Smith JK, Jewells V, Gilmore JH. 2009. Temporal and spatial development of axonal maturation and myelination of white matter in the developing brain. *Am J Neuroradiol*. 30:290–296.

Geng X, Gouttard S, Sharma A, Gu H, Styner M, Lin W, Gerig G, Gilmore JH. 2012. Quantitative tract-based white matter development from birth to age 2 years. *Neuroimage*. 61:542–557.

Gilmore JH, Knickmeyer RC, Gao W. 2018. Imaging structural and functional brain development in early childhood. *Nat Rev Neurosci*. 19:123–137.

Gilmore JH, Schmitt JE, Knickmeyer RC, Smith JK, Lin W, Styner M, Gerig G, Neale MC. 2010. Genetic and environmental contributions to neonatal brain structure: a twin study. *Hum Brain Mapp*. 31:1174–1182.

Gilmore JH, Shi F, Woolson SL, Knickmeyer RC, Short SJ, Lin W, Zhu H, Hamer RM, Styner M, Shen D. 2012. Longitudinal development of cortical and subcortical gray matter from birth to 2 years. *Cereb Cortex*. 22:2478–2485.

Girault JB, Cornea E, Goldman BD, Knickmeyer RC, Styner M, Gilmore JH. 2019. White matter microstructural development and cognitive ability in the first 2 years of life. *Hum Brain Mapp*. 40:1195–1210.

Girault JB, Langworthy BW, Goldman BD, Stephens RL, Cornea E, Reznick JS, Fine J, Gilmore JH. 2018. The predictive value of developmental assessments at 1 and 2 for intelligence quotients at 6. *Intelligence*. 68:58–65.

Guillery RW. 2005. Is postnatal neocortical maturation hierarchical? *Trends Neurosci*. 28:512–517.

Kinney H, Brody A, Kloman A, Gilles S. 1988. Sequence of central nervous system myelination in human infancy. *J Neuropathol Exp Neurol*. 47:217–234.

Knickmeyer RC, Gouttard S, Kang C, Evans D, Wilber K, Smith JK, Hamer RM, Lin W, Gerig G, Gilmore JH. 2008. A structural MRI study of human brain development from birth to 2 years. *J Neurosci*. 28:12176–12182.

Knickmeyer RC, Xia K, Lu Z, Ahn M, Jha SC, Zou F, Zhu H, Styner M, Gilmore JH. 2016. Impact of demographic and obstetric factors on infant brain volumes: a population neuroscience study. *Cereb Cortex*. 27:5616–5625.

Krogsrud SK, Fjell AM, Tamnes CK, Grydeland H, Mork L, Due-Tønnessen P, Bjørnerud A, Sampaio-Baptista C, Andersson J, Johansen-Berg H *et al*. 2016. Changes in white matter microstructure in the developing brain-a longitudinal diffusion tensor imaging study of children from 4 to 11 years of age. *Neuroimage*. 124:473–486.

Kuhl PK, Stevens E, Hayashi A, Deguchi T, Kiritani S, Iverson P. 2006. Infants show a facilitation effect for native language phonetic perception between 6 and 12 months. *Dev Sci*. 9:13–21.

Lebel C, Beaulieu C. 2009. Lateralization of the arcuate fasciculus from childhood to adulthood and its relation to cognitive abilities in children. *Hum Brain Mapp*. 30: 3563–3573.

Lebel C, Beaulieu C. 2011. Longitudinal development of human brain wiring continues from childhood into adulthood. *J Neurosci*. 31:10937–10947.

Lebel C, Deoni S. 2018. The development of brain white matter microstructure. *Neuroimage*. 182:207–218.

Lebel C, Treit S, Beaulieu C. 2019. A review of diffusion MRI of typical white matter development from early childhood to young adulthood. *NMR Biomed*. 32:e3778.

Lee SJ, Steiner RJ, Luo S, Neale MC, Styner M, Zhu H, Gilmore JH. 2015. Quantitative tract-based white matter heritability in twin neonates. *Neuroimage*. 111:123–135.

Lee SJ, Steiner RJ, Yu Y, Short SJ, Neale MC, Styner M, Zhu H, Gilmore JH. 2017. Common and heritable components of white matter microstructure predict cognitive function at 1 and 2 years. *Proc Natl Acad Sci. U S A* 114:148–153.

Lee S, Zhang J, Neale MC, Styner M, Zhu H, Gilmore JH. 2019. Quantitative tract-based white matter heritability in 1-and 2-year-old twins. *Hum Brain Mapp*. 40:1164–1173.

Liu Z, Wang Y, Gerig G, Gouttard S, Tao R, Fletcher T, Styner M. 2010. Quality control of diffusion weighted images. *Proc SPIE–the Int Soc Opt Eng*. 7628:76280J.

Mabbott DJ, Noseworthy M, Bouffet E, Laughlin S, Rockel C. 2006. White matter growth as a mechanism of cognitive development in children. *Neuroimage*. 33:936–946.

Mishra V, Cheng H, Gong G, He Y, Dong Q, Huang H. 2013. Differences of inter-tract correlations between neonates and children around puberty: a study based on microstructural measurements with DTI. *Front Hum Neurosci*. 7:721.

Nagy Z, Westerberg H, Klingberg T. 2004. Maturation of white matter is associated with the development of cognitive functions during childhood. *J Cogn Neurosci*. 16:1227–1233.

Nelson CA, Zeanah CH, Fox NA, Marshall PJ, Smyke AT, Guthrie D. 2007. Cognitive recovery in socially deprived young children: the Bucharest early intervention project. *Science*. 318:1937–1940.

Oguz I, Farzinfar M, Matsui J, Budin F, Liu Z, Gerig G, Johnson HJ, Styner M. 2014. DTIPrep: quality control of diffusion-weighted images. *Front Neuroinform*. 8:4.

Pascalis O, De Haan M, Nelson CA. 2002. Is face processing species-specific during the first year of life? *Science*. 296:1321–1323.

Paydar A, Fieremans E, Nwankwo JI, Lazar M, Sheth HD, Adisetiyo V, Helpern JA, Jensen JH, Milla SS. 2014. Diffusional kurtosis imaging of the developing brain. *Am J Neuroradiol*. 35:808–814.

Pecheva D, Yushkevich P, Batalle D, Hughes E, Aljabar P, Wurie J, Hajnal JV, Edwards AD, Alexander DC, Counsell SJ *et al*. 2017. A tract-specific approach to assessing white matter in preterm infants. *Neuroimage*. 157:675–694.

Qiu A, Mori S, Miller M. 2015. Diffusion tensor imaging for understanding brain development in early life. *Annu Rev Psychol*. 66:853–876.

Simmonds DJ, Hallquist MN, Asato M, Luna B. 2014. Developmental stages and sex differences of white matter and behavioral development through adolescence: a longitudinal diffusion tensor imaging (DTI) study. *Neuroimage*. 92:356–368.

Smith SM. 2002. Fast robust automated brain extraction. *Hum Brain Mapp*. 17:143–155.

Smith SM, Jenkinson M, Johansen-Berg H, Reuckert D, Nichols TE, Mackay CE, Watkins KE, Ciccarelli O, Cader MZ, Matthews PM *et al*. 2006. Tract-based spatial statistics: voxelwise analysis of multi-subject diffusion data. *Neuroimage*. 31:1487–1505.

Stephens RL, Langworthy B, Short SJ, Goldman BD, Girault JB, Fine JP, Reznick JS, Gilmore JH. 2018. Verbal and nonverbal predictors of executive function in early childhood. *J Cogn Dev*. 19:182–200.

Steven AJ, Zhuo J, Melhem ER. 2014. Diffusion kurtosis imaging: an emerging technique for evaluating the microstructural environment of the brain. *AJR Am J Roentgenol*. 202:W26–W33.

Tamnes CK, Roalf DR, Goddings AL, Lebel C. 2017. Diffusion MRI of white matter microstructure development in childhood

and adolescence: methods, challenges and progress. *Dev Cogn Neurosci*. 33:161–175.

Thomason ME, Thompson PM. 2011. Diffusion imaging, white matter, and psychopathology. *Annu Rev Clin Psychol*. 7:63–85.

Tsivilis D, Vann SD, Denby C, Roberts N, Mayes AR, Montaldi D, Aggleton JP. 2008. A disproportionate role for the fornix and mammillary bodies in recall versus recognition memory. *Nat Neurosci*. 11:834–842.

Verde AR, Budin F, Berger J-B, Gupta A, Farzinfar M, Kaiser A, Ahn M, Johnson H, Matsui J, Hazlett HC *et al*. 2014. UNC-Utah NA-MIC framework for DTI fiber tract analysis. *Front Neuroinform*. 7:51.

Vos SB, Jones DK, Viergever MA, Leemans A. 2011. Partial volume effect as a hidden covariate in DTI analyses. *Neuroimage*. 55:1566–1576.

Werker JF, Tees RC. 1984. Cross-language speech perception: evidence for perceptual reorganization during the first year. *Infant Behav Dev*. 7:49–63.

Wilkinson M, Lim AR, Cohen AH, Galaburda AM, Takahashi E. 2017. Detection and growth pattern of arcuate fasciculus from newborn to adult. *Front Neurosci*. 11:389.

Winklewski PJ, Sabisz A, Naumczyk P, Jodzio K, Szurowska E, Szarmach A. 2018. Understanding the physiopathology behind axial and radial diffusivity changes—what do we know. *Front Neurol*. 9:92.

Wolff JJ, Gu H, Gerig G, Elison JT, Styner M, Gouttard S, Botteron KN, Dager SR, Dawson G, Estes AM *et al*. 2012. Differences in white matter fiber tract development present from 6 to 24 months in infants with autism. *Am J Psychiatry*. 169: 589–600.

Zhang H, Schneider T, Wheeler-Kingshott CA, Alexander DC. 2012. NODDI: practical in vivo neurite orientation dispersion and density imaging of the human brain. *Neuroimage*. 61:1000–1016.